Processing and Characterization of Silicon Nitride for Rapid and Low-Level Detection of Water Pathogens

A Senior Project

presented to

the Faculty of the Materials Engineering Department

California Polytechnic State University—San Luis Obispo

In Partial Fulfillment

of the Requirements for the Degree

Bachelor of Science

By

Arielle Buchanan and Logan Chai

June 2022

Abstract

Water sanitation is a serious issue affecting the lives of many, and methods for assessing water cleanliness have been a major research interest for decades. Rapid and accurate water pathogen detection methods that can be performed in field applications have been a growing research focus, especially in low-income countries most affected by poor water quality. Silicon nitride was explored as a material for colorimetric water-pathogen sensing due to the large body of knowledge around its processing, and its isoelectric point. A bioassay of chlorophenol red-β-D-galactopyranoside (CPRG) and β-galactosidase (β-gal) enzymes with *Escherichia coli (E. coli)* bacteria was used to examine the colorimetric reading produced by electrostatic binding of *E. coli* to the surface of etched silicon nitride samples. Silicon nitride samples were produced by etching a pattern of repeating 250 μm side-length squares onto a silicon nitride wafer for different etch durations using buffered oxide etch (BOE) to increase its surface area for *E. coli* binding. Roughness and surface area were measured via profilometry and Brunauer-Emmett-Teller (BET) analysis, respectively. After being submersed in the bioassay, the colorimetric readout was measured via spectrophotometry. Some statistically significant differences were observed for larger samples at longer etch-times compared with control values, though this trend was inconsistent. Further research should be conducted to investigate methods for producing samples with sufficient surface area for adequate and consistent bacteria binding.

Table of Contents

I. Background

1. Introduction

In 2003, the Secretary-General Kofi Annan indicated that 80% of deaths and illnesses in the world are water-related (Annan, 2003). A large proportion of these deaths are caused by drinking water sources contaminated with human pathogens, which are defined as "microbial or parasite species that can infect and [are] capable of causing disease in humans under natural transmission conditions" (Woolhouse, 2006). Waterborne pathogens pose a danger to public health, killing more than 2.2 million people annually as of 2015 (Ramirez-Castillo, 2015). According to the World Health Organization (WHO), 28.9% of the global population in 2017 went without access to safely managed drinking-water sources, defined as water sources "free from faecal and priority chemical contamination" and located within 30 minutes round trip of a premises (WHO, 2019). Studies on the link between water sanitation and health risks by the WHO have indicated a correlation between poor sanitation and transmission of serious diseases like cholera, diarrhea, dysentery, hepatitis A, typhoid, and polio. Several of these diseases are largely preventable and affect low-income countries in significantly greater proportions (WHO, 2019). The WHO also estimates that less access to clean water sources poses a safety risk as people are forced to make longer, more difficult journeys to collect water; additionally, time spent acquiring water decreases overall economic productivity of a region and can perpetuate poverty. Water sanitation is not merely a matter of health but also of overall livelihood, and with such a large percentage of the global population lacking access to clean water, this is a serious ethical issue requiring investigation from the research community.

2. Current Detection Methods

A. Molecular-Based Detection

Considering the serious nature of waterborne pathogens, there has been significant work in developing detection methods for identifying contaminated water sources that pose a risk to public health. Diagnoses of water sources are effective for deciding water treatment methods to prevent the spread of diseases from waterborne pathogens (Ramirez-Castillo, 2015). There is currently no single detection method for understanding and analyzing the presence of all

parasites, bacteria, viruses, and chemical contaminants that lead to major health risks. This is largely due to the extensive diversity and evolving nature of human pathogens (Woolhouse, 2006). As of 2006, there are at least 1,407 recognized species of human pathogens all varying in phenotypic and genetic characteristics; of these species, bacteria comprise the largest proportion at 538 species (Ramirez-Castillo, 2015). This poses a particularly difficult challenge to water pathogen detection research, as methods are limited not only by the taxonomic differences in human pathogens but also the generally low concentration of pathogens in much larger volumes of water being tested. Despite these challenges, there are a plethora of current methods for detecting the presence of pathogens in water sources that provide sufficient data to conclusively determine their safety, though the majority require expensive laboratory equipment that pose a different challenge to accessibility.

One of the most commonly-used methods for water pathogen detection is polymerase chain reaction (PCR) (Ramirez-Castillo, 2015). This technique involves amplifying specific DNA fragments using a cyclic denaturation, annealing, and polymerization process that allows for detection of targeted sequences found in specific pathogens (Mandal, 2011). Several variations of the PCR technique exist to detect specific genes characteristic of different water pathogens, including PCR methods focused on targeting mRNA sequences. Other techniques like oligonucleotide DNA micro-arraying and pyrosequencing are also based on analysis of DNA to observe targeted sequences (Ramirez-Castillo, 2015). Oligonucleotide DNA microarrays are a type of genomic technology that analyzes for expression of particular genes and monitors how expression reacts to different environments (Zhou, 2003). Pyrosequencing is another technique that relies on bioluminescence from pyrophosphates released in proportion to nucleotides' incorporation into a short DNA sequence; this technique allows for isolation and genome sequencing for targeted sequences (Ahmadian, 2006). In addition to DNA-focused methods, researchers can also use immunological detection based on observation of antigen interactions with introduced antibodies (Iqbal, 2000).

B. Limitations of *in-vitro* Analysis

These methods and many others are useful for detection of specific pathogens in different scenarios. However, one shared limitation is that all these methods require analysis *in-vitro*, in a

laboratory or somewhere with access to sensing technology. This makes it difficult to perform a diagnostic test in the field and limits access to detection technology in low-income countries where waterborne pathogens are most prevalent. Field application necessitates development of a portable assay that can perform rapid detection with minimal materials and little to no technological equipment for analysis of results. One example of a more field-friendly assay is fluorescence *in situ* hybridization (FISH), which allows for tagging different genetic components using fluorophores that can be analyzed to identify different gene expression patterns (ThermoFisher, 2021). However, this method is still limited even in field applications as it requires tyramide signal amplification (TSA) imaging technology to observe and analyze fluorescence signals, which are not easily accessible in the field. Recent research has aimed to develop an *in situ* method that allows for optical analysis of results with the naked eye to increase accessibility of rapid detection to low-income countries where water sanitation is a more serious issue.

3. Recent Research

A. Colorimetric Bacteria Detection

Water pathogens contaminating drinking water sources are nearly all gastrointestinal — or enteric — microbial or parasite organisms, with few exceptions like *B. pseudomallei*, hepatitis E, *Toxoplasma gondii*, or *Schistosoma spp*. which cause skin infections or infectious hepatitis (Ramirez-Castillo, 2015). Because of this, detection methods for water pathogens may focus on screening for fecal matter, the primary source for enteric pathogens. One method studied by Oscar Miranda *et al.* examined the viability and efficacy of a positively-charged nanoparticle as a sensor for detecting the presence of enteric coliform bacteria (Miranda, 2011). This method was founded on the concept of Coulombic attraction between the positively-charged nanoparticle and the negatively-charged coliform bacteria, which has negatively-charged cell walls. The system contains two bioparticles: the enzyme ß-galactosidase (ß-gal) and the dye chlorophenol red-ß-D-galactopyranoside (CPRG).

ß-gal is an anionic enzyme that converts lactose to allolactose and hydrolyzes lactose into glucose and galactose; allolactose is an inducer that promotes gene expression in cells, and glucose and galactose are readily accessible sugars that can be broken down to produce energy,

which makes it a useful enzyme for cells (Juers, 2012). ß-gal is also known to hydrolyze galactopyranoside molecules to release their color compound; in the case of this system, ß-gal hydrolyzes CPRG which turns the system red. Once a microbe is introduced, however, ß-gal is consumed due to its role in performing the aforementioned necessary functions for cells that promote survival. In a system with ß-gal, CPRG, and a microbe, the ß-gal is consumed by the microbe and the system does not turn red. This method uses *E. coli* bacteria since they are one of the most common enteric bacteria, and while most strains are non-pathogenic, their presence in water indicates the presence of fecal matter and other potentially pathogenic microbes or parasites.

When a positively-charged nanoparticle is introduced to the system, the negatively-charged bacteria are Coulombically attracted to the particle and are unable to consume the free-floating ß-gal, which then hydrolyze the CPRG and turn the system red. Similarly, because ß-gal is also anionic, if there were no pathogens present the ß-gal would be Coulombically attracted to the nanoparticle, inhibiting hydrolysis of the CPRG and maintaining the original color of the system (Miranda, 2011). This means ß-gal and the negatively-charged bacteria compete in Coulombic attraction to the positively-charged nanoparticle; attraction is proportional to the magnitude of each charge. Since bacteria are significantly larger than ß-gal molecules, they would be more strongly attracted to the positive charge of the nanoparticle than the ß-gal; therefore the negatively-charged bacteria competes more strongly when present and is more likely to take up nanoparticle surface area first. This interaction between the bioparticles, the positively-charged nanoparticle, and the cationic pathogen microbes are illustrated in Figure 1.

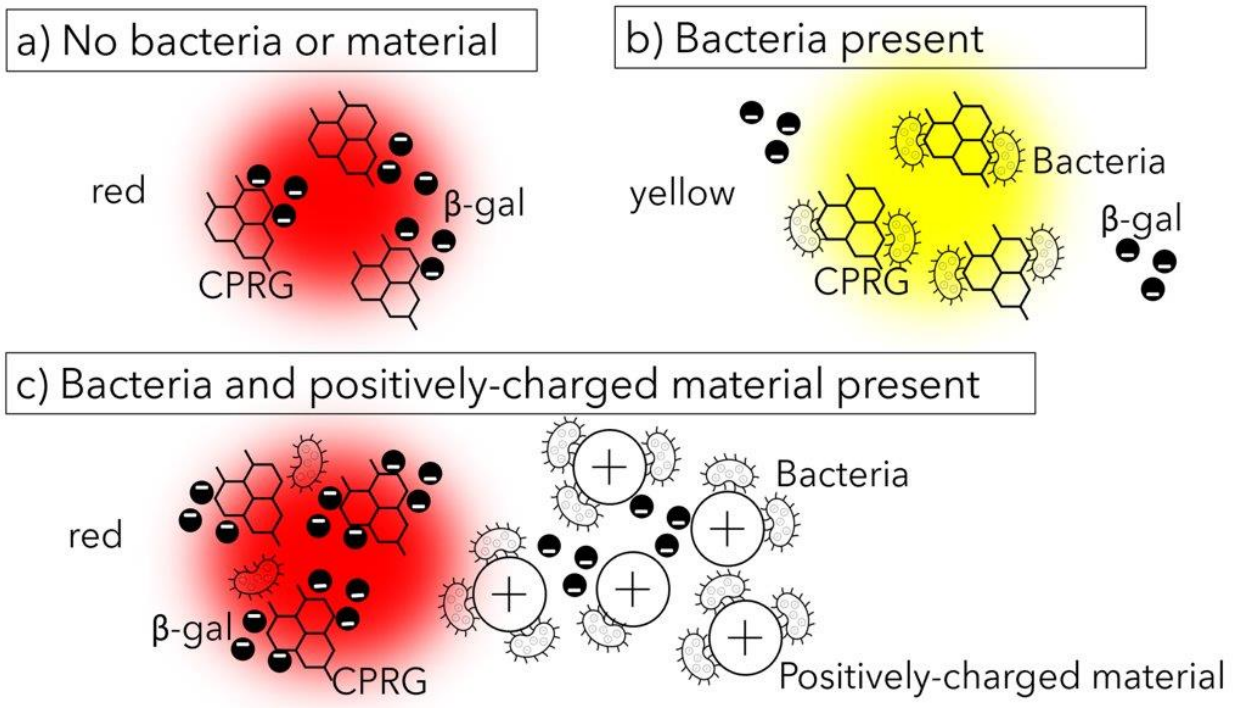

Figure 1. (a) Red color produced from enzymatic interactions of β-gal and CPRG; (b) bacteria inhibiting enzymatic activity between β-gal and CPRG; (c) bacteria and β-gal electrostatically attracted to surface of positively-charged material, with bacteria outcompeting β-gal which enzymatically interacts with CPRG uninhibited, producing red color.

This method also provides a visual indicator of the concentration of *E. coli* present. Because the bacteria has a greater magnitude of charge driving its attraction to the positive nanoparticle in comparison with ß-gal, it is more likely to attach to the surface of the nanoparticle first and use up surface area; the remaining ß-gal that is unable to attach to the nanoparticle due to surface area unavailability hydrolyzes the CPRG. Higher concentrations of *E. coli* take up greater nanoparticle surface area, allowing more ß-gal to hydrolyze CPRG that results in a greater release of red color compounds. Hence, a more intense red color indicates a greater concentration of bacteria. The study by Miranda *et al*. examined these color changes at different concentrations of bacteria by measuring the release of red color compounds from CPRG as the kinetic absorbance of ß-gal enzymes at different bacteria concentrations as well as by visual observation using images taken 10 minutes after introduction of different concentrations of bacteria into the

system. Responses were compared against a control system that had no bacteria. These results are illustrated in Figure 2.

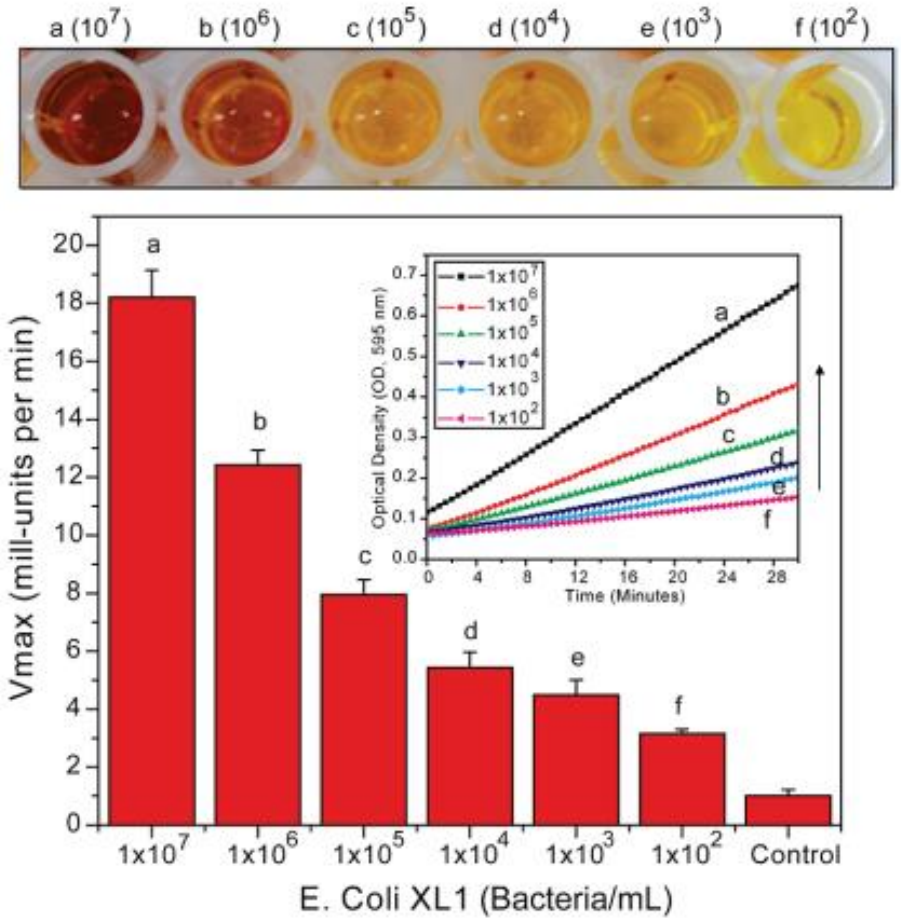

Figure 2. (Top) Visual color changes from release of red compound from CPRG at varying concentrations of E. coli. (Bottom) Plot of kinetic absorbance of ß-gal vs E. coli concentration.

This particular study also developed a test strip to use in field applications where the system was contained in a strip of grade GF/B (pore sizes of 1 μm) binder-free microfiber filter paper and compared with a range of colors developed from previous experimental data; using the test strip yielded results that were able to detect as low as 1,000 bacteria per mL (Miranda, 2011). This value is well within the range of the median infectious dose (ID50) for enteropathogenic,

enterotoxigenic, and enteroinvasive *E. coli* strains, though this would not detect the ID50 for enterohemorrhagic *E. coli* (FDA, 2012). This technique is more feasible for *in-situ* field applications in low-income countries where there is limited access to complex and costly technology for analysis of detection methods for water pathogens.

Similar research has been conducted to confirm the reliability of Coulombic attraction as a method for capturing bacteria in detection assays. Other research has indicated the success of positively-charged amine-terminated polyamidoamine dendrimers in Coulombically capturing negatively-charged bacteria with a detection limit of 10,000 cells per mL (Ji, 2004). Similarly, cetyltrimethylammonium bromide (CTAB)-functionalized gold nanorods were observed to form a monolayer on *B. cereus* by Coulombic attraction, further validating the electrostatic interactions between positively-charged nanoparticles and negatively-charged bacteria (Berry, 2005). This study by Miranda *et al.* and other studies used various functionalized gold nanoparticles to detect bacteria and other pathogenic species (Miranda, 2011).

B. Cost Limitations of Current Nanoparticle Materials

One major limitation of this method, however, is that gold is one of the most expensive materials available at $57.36 per gram which presents yet another challenge to developing a detection method that is accessible for low-income regions (Monex, 2021). One consideration is silicon as a viable candidate to substitute the gold nanoparticles while maintaining strong electrostatic interactions with negatively-charged bacteria. Silicon is significantly cheaper than gold at $0.50 per gram and has a wide range of uses and known manufacturing methods (Holmes, 2016).

C. Surface Processing of Silicon to Produce Positively-Charged Samples

Silicon is the most common material used in semiconductors today, and thus has a well-developed set of fabrication processes (Hitachi, 2021). Unfortunately, one of the main issues to consider when using silicon is that it has a net neutral charge in an isolated environment, so it does not drive Coulombic attraction in an unaltered state. One proposed idea was to positively dope silicon using a boron dopant in order to produce a positive surface charge. However,

doping a semiconductor does not change its overall electric charge, as it only changes the majority charge carrier type which are fixed to dopants (Halbleiter, 2021). As such, other methods to induce an electric charge in silicon must be considered. One potential option is to modify the isoelectric point (IEP) of silicon. The IEP of a material is the pH at which the material has a net neutral charge; if silicon is modified so it has an IEP above the pH of water, a net positive surface charge can be produced (Kosmulski, 2016). There are a few ways to modify silicon to do this: the surface of the silicon can be hydroxylated and sulfates can be attached in order to tune the IEP, or silicon can be modified by reacting it with oxygen or nitrogen to form oxides and nitrides, respectively (van der Maaden, 2014). This modification method is shown in Figure 3. These materials already show IEPs that diverge from the neutral pH of 7, and as such can be used as an alternative. Silicon nitride (Si_3N_4) has shown a usable IEP, ranging from 7-9 pH at 25ºC (Lewis, 2004).

In order to fabricate a Si_3N_4 sample, a several methods of production are available. By powdering silicon and then heating it above 1413ºC in a nitrogen environment, Si_3N_4 and a few unstable nitrides can be formed on a silicon substrate (Okamoto, 2005). Alternatively, chemical vapor deposition (CVD) can be used to deposit a layer of Si_3N_4 on a silicon substrate (Riley, 2004). Deposition of nitrides can be seen in Figure 4 as the rougher textured components on top of a smoother silicon substrate layer.

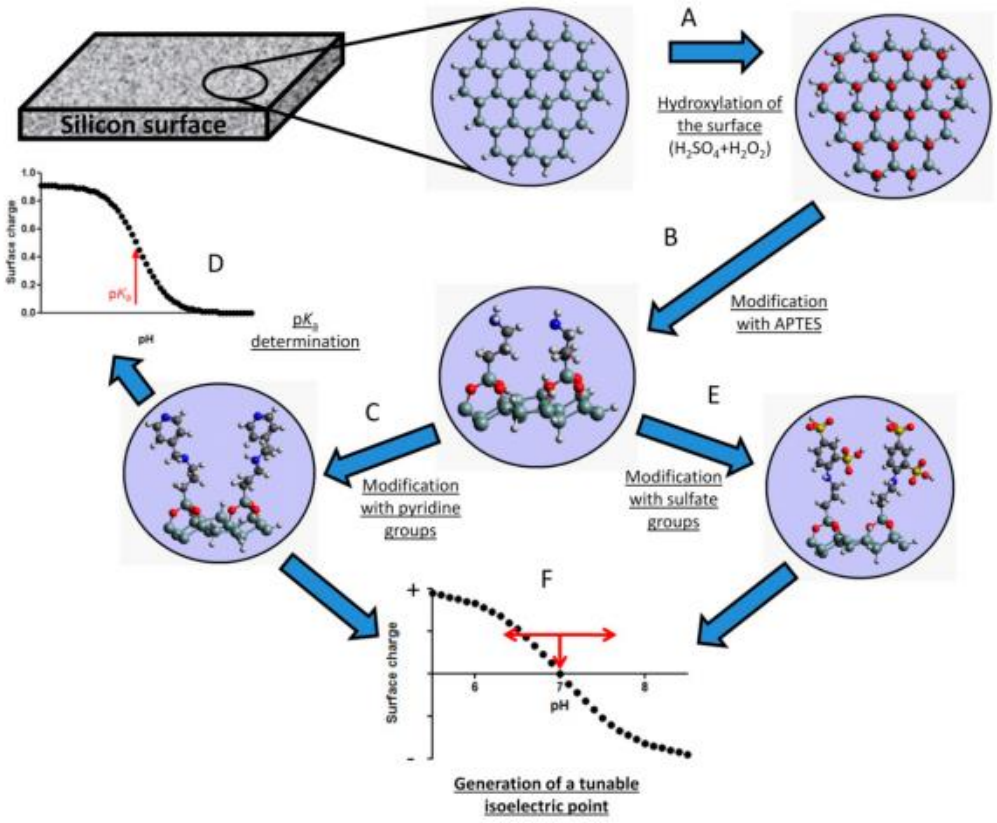

Figure 3. Modification of a silicon substrate's isoelectric point via hydroxylation and further modification with sulfate groups (van der Maaden, 2014)

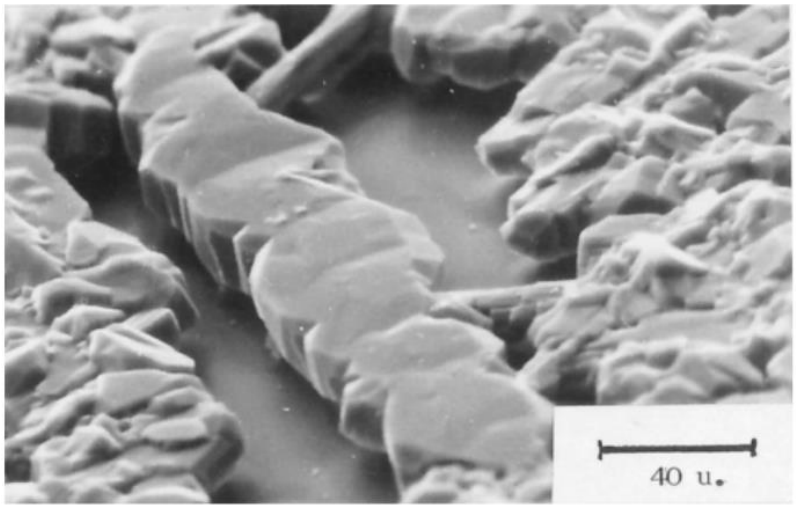

Figure 4. Formation of Si_3N_4 on a silicon substrate (Riley, 2004)

The advantage of this method is the flexibility of the processing conditions; it can be done in a low pressure environment such as low pressure chemical vapor deposition (LPCVD) at higher temperatures, or at lower temperatures in vacuum conditions, such as by plasma enhanced chemical vapor deposition (PECVD). These methods are readily available even in Class 1000 cleanrooms. Theoretically, a layer as thin as 100 μm should be sufficient to produce a charged double layer on the surface of the material (Riley, 2004). Wang *et al*. researched the influence of various cleanroom processes and machining effects on the chargeability and charge stability of Si_3N_4; a smaller amount of Si_3N_4 results in decreased charge stability, so increasing the thickness of the deposited layer may produce a larger surface charge, resulting in greater Coulombic attraction. Similarly, maximizing the surface area of the silicon nitride substrate can achieve increased Coulombic attraction. Some methods of surface roughening that may result in higher substrate surface area include wet etching using different etchant recipes with strong acids, or dry etching methods like reactive ion etching (RIE) or laser ablation (Leber, 2016). Surface roughening processes are highly dependent on available manufacturing capabilities, but generally it has been found that different processes produce variable results that are dependent on both the environment and the material (Leber, 2016). For silicon, wet etching is most commonly used due to the straightforward process of applying an acid-based etchant to the surface and because most laboratories can support this method, making it the most accessible surface roughening technique.

4. Research Questions

In order to identify whether Si_3N_4 can be used as a successful agent for detecting negatively-charged bacteria using ß-gal and CPRG, various surface textures will be produced by etching Si_3N_4 with buffered oxide etch (BOE) for various durations and measuring samples of varying mass. The research questions pursued are:

- How does varying the etch duration of a uniform Si_3N_4 layer deposited on a silicon substrate impact the etch depth and subsequent surface roughness?
- What is the relationship of etch duration and the resulting surface area with sample size?

- How do these effects impact the colorimetric readout when exposed to the same concentrations of ß-gal and CPRG at room temperature in phosphate buffer solution without bacteria?
- How does varying the concentration of *E. coli* bacteria affect the intensity of the colorimetric readout?

II. Methods

1. Wafer Processing

Silicon wafers with a deposited nitride layer were used for this project; they were manufactured using low-pressure chemical vapor deposition (LPCVD) by University Wafers and was stated to have an average silicon nitride thickness of 149 nm. The wafers were manufactured in March 2007, so it was first necessary to examine them for potential degradation from age. However, this was unlikely since nitride is highly stable at room temperature and pressure, and the wafers were kept in the Cal Poly Microfabrication Lab since their manufacture date. A 10-point optical Filmetrics F20 apparatus in the Cal Poly Microfabrication Lab was used to check the thickness of the nitride layer. It indicated an average nitride thickness of around 148 nm, confirming that the wafers suffered no degradation for the purposes of this project and that age would not be a consideration in performance.

Simple and relatively fast fabrication methods were selected due to the processing limitations of the Cal Poly Microfabrication Lab and to increase the availability of the Microfabrication Lab for other research groups. A wet etching technique was selected for increasing the surface area of the Si_3N_4 layer for ß-gal and *E. coli* binding.

The wafers were first patterned using a checkerboard mask with square cells with a 250 µm edge length to promote a uniformly rough surface, as shown in Figure 5.

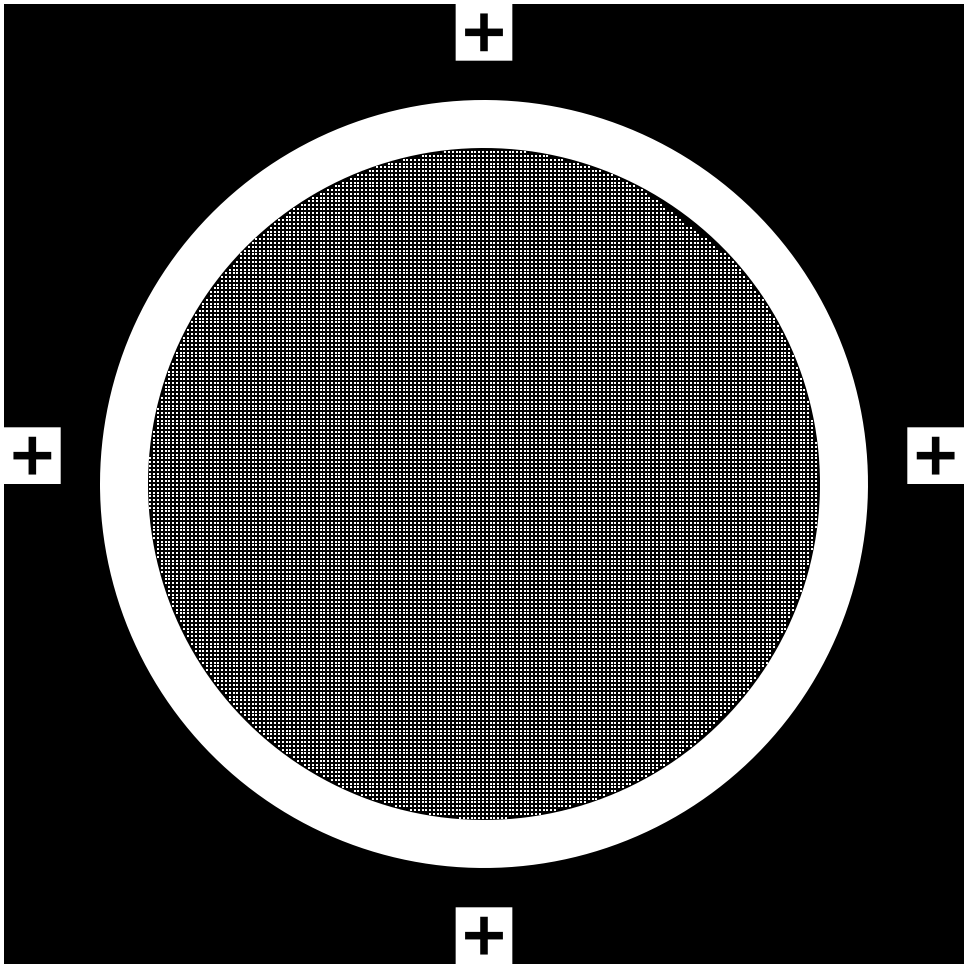

Figure 5. Checkerboard pattern with 250 µm cells for a 6" x 6" mask.

To vary the surface area, the wafers were wet etched for increasing durations to increase the depth of the etched pattern. Buffered oxide etchant (BOE), a hydrofluoric-acid based etchant, was used in a 1:6 volume ratio of hydrofluoric acid (HF) to ammonium fluoride (NH_4F) to etch the wafers at a rate of 6 nm/min at 21ºC for 1 hr, 1.5 hrs, and 2 hrs. The etch rate was extrapolated from previous literature data (Burham, 2016) on the etch rate of silicon nitride using a 1:6 volume ratio of HF: NH_4F, as depicted in Figure 6.

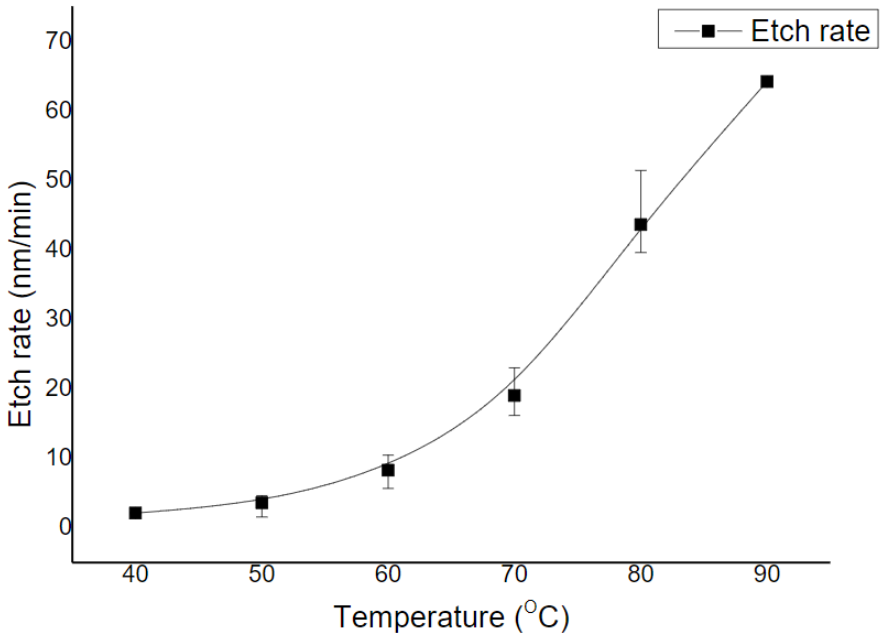

Figure 6. Etch rate of nitride at varied temperatures of BOE (Burham, 2016)

The experiment was conducted according to approved safety protocols and procedures with supervision of the Microfabrication Lab director and co-director. The wafers were first cleaned and patterned with the checkboard mask using soft photolithography with a positive photoresist. Cleaning was done by immersing wafers in piranha solution (a mixture of 75% by volume sulfuric acid and 25% by volume hydrogen peroxide) at 70ºC for 10 min at an acid bench, and then quench rinsed in deionized water and dried using a spin rinse dryer (SRD). Then the positive photoresist was spun onto the wafers according to the sequence found in Table I.

Table I: Shipley S1813 Resist Process with hexamethyldisilazane (HMDS) primer 80/20

Step	Process	Time (sec)	Speed (rpm)
1	Post dispense HMDS	30	300
2	Spread/Dry HMDS	20	3000
3	Dispense resist	30	3000
4	Spread Resist	30	600
5	Planarize Resist	20	4000
6	Slow and stop	5	300

Once the photoresist was deposited, wafers were soft baked at 115ºC for 120 seconds and prepared for mask transfer. The mask was placed in a manual mask aligner (GAMM aligner) in the photolithography area of the clean room, and the wafer was aligned and exposed using the GAMM aligner's preprogrammed exposure sequence, which used proximity contact and exposed the wafer to UV light for 20 seconds to transfer the mask pattern onto the silicon nitride wafer. Exposed wafers were then developed in the developing hood by immersing them in tetramethylammonium hydroxide (TMAH) for 3 min and rinsed using deionized water, followed by a hard bake at 150ºC for 60 sec before being moved to the acid bench for etching.

For etching, a step-etch process was used to verify etch rates and compare etch profiles side-by-side. One wafer was loaded into a Teflon single wafer holder and marked into thirds as a position reference for each etch step. Steps were set according to etch duration times of 1 hr, 1.5 hrs, and 2 hrs to reflect corresponding etch depths; for the first step, the entire wafer was submerged for 0.5 hr, then moved to the second step and etched for another 0.5 hr, then moved to the last step and etched for an additional 1 hr. The wafer was then quench-rinsed in deionized water and dried using the SRD, then resist-stripped at 60ºC for 10 min using Microposit Remover 1165. It was again quench-rinsed and dried before being prepared for characterization.

A Mitutoyo SJ-201 profilometer was used to determine the surface roughness of the wafers. The profilometer was calibrated beforehand to ±2 μm of a reference standard. Due to the hand-held nature of the profilometer, samples were held down with tape to ensure no sample movement during testing. The measurements were 0.8 mm per measurement, with five repetitions each to ensure precision of results. Three trials were then performed for each wafer etch time, as well as for a unetched wafer as a reference.

To determine qualitative effects, scanning electron microscopy (SEM) was utilized to image the surface of the wafer to compare etch depth profiles. SEM was conducted through the Cal Poly MATE department using a high vacuum setting. The wafer was then cleaved into the three etch-step sections as shown in Figure 7, and then subsequently cleaved into samples of different three sizes (3 mm x 4 mm, 4 mm x 4 mm, and 5 mm x 4 mm) to test for consistency of results across sample dimensions.

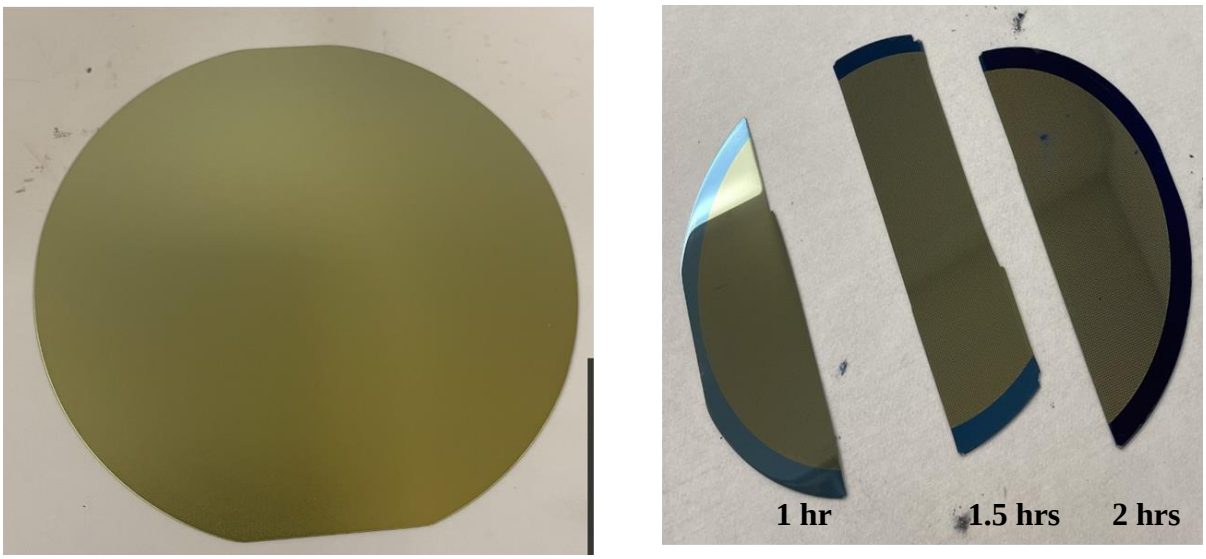

Figure 7. Unetched wafer (left) and silicon nitride wafer post-step etching, cleaved into three segments to separate etch steps (right).

Scanning electron microscope (SEM) images were taken of the surfaces of the samples using a working distance of 10 mm with samples tilted at an angle of 10 degrees with respect to the surface of the sample mount to exaggerate surface features for visibility; profile images were taken by examining cross-sections of the wafer. After SEM imaging, quantitative surface area characterization was performed using Brunauer-Emmett-Teller (BET) measurements. The Quantachrome Monosorb Rapid Surface Area Analyzer MS-22 was used to take BET surface area measurements of the etched samples and compared with surface area measurements of an unetched wafer as a reference. A Mitutoyo SJ-201 profilometer was also used to compare the roughness of the etched samples with an unetched reference wafer by running a probe over the sample surface 5 times and taking the arithmetic average roughness, or R_a, of these measurements over a length of 2 mm for each scan. Once characterization was completed, samples were prepared for biological testing.

2. Biological Testing

All biological testing was performed in a biosafety Level 2 pathogen lab at Cal Poly according to proper safety protocols and procedures; previous Cal Poly research students Sydney Fultz-Waters and Danica Wong had conducted research using CPRG and ß-gal for broader material

testing, and their procedure was modified and used for this experiment. According to the modified procedure, preparation of pathogenic water cells required two days to prepare for testing with silicon nitride samples. The first day of preparation was required for making an overnight culture of *E. coli* to grow for 24 hours before making dilutions. Over the course of the experiment, *E. coli* was maintained by streak-plating every two days on tryptic soy agar (TSA) media plates made from a mixture of tryptic soy broth (TSB) and agar; this process is depicted in Figure 8.

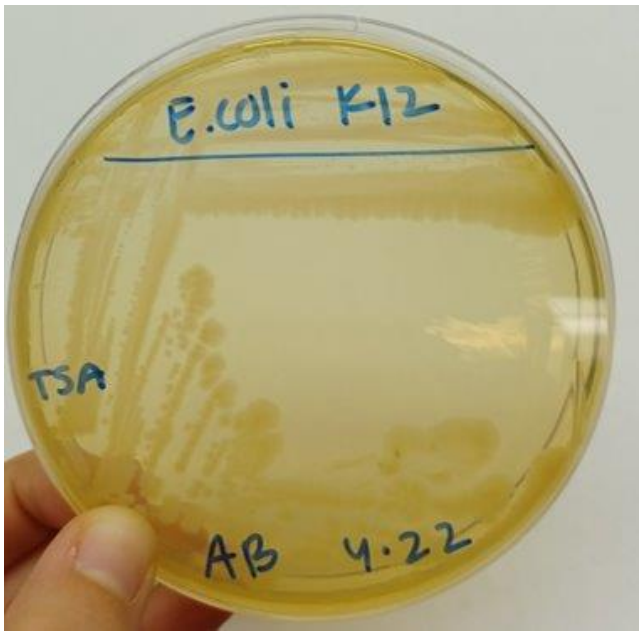

Figure 8. E. coli cultures streak-plated on a TSA media plate after 48 hours.

For the experiment preparation, the overnight culture of *E. coli* was prepared by culturing in TSB at a room temperature of 29ºC for 24 hours. Stock solutions of ß-gal and CPRG were also prepared during the first day with phosphate buffered solution (PBS). On the second day, seven dilutions were prepared to test colorimetric response to decreasing concentrations of *E. coli* and to determine the efficacy of silicon nitride at detecting lower levels of pathogens present in water samples; dilutions were compared with an undiluted concentration of *E. coli* as a reference. Dilution concentration counts were verified using enumeration, a biological technique where 100

µL of a dilution is spread into a thin layer on a TSA media plate and allowed to grow for 48 hours (Figure 9); colonies are then counted to calculate dilution concentration.

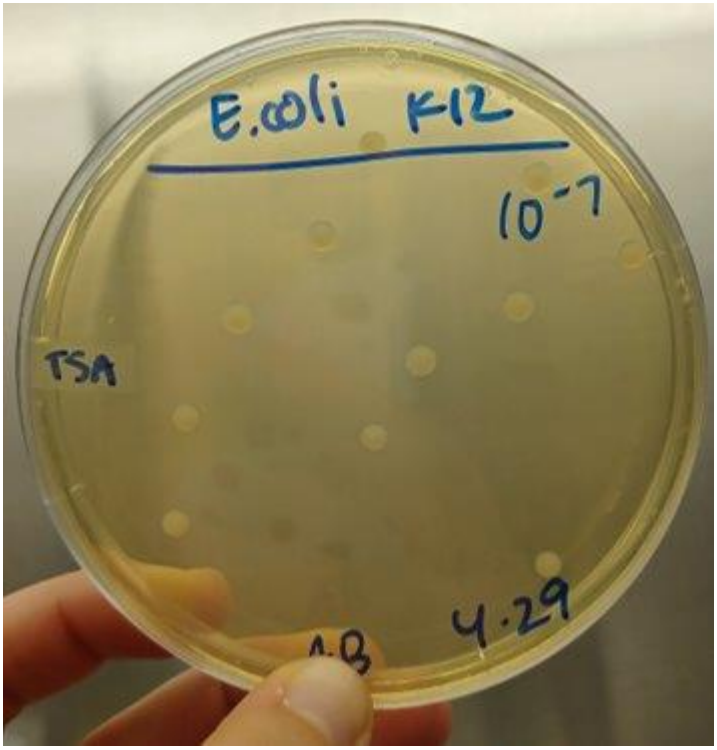

Figure 9. Enumeration of the highest dilution of E. coli on a TSA media plate; 11 colonies were counted, verifying a dilution concentration of $1.1x10^2$ CFU/mL and an undiluted concentration of the original overnight culture of $1.1x10^9$ CFU/mL

CPRG and β-gal stock were prepared on the same day as the *E. coli* cultures so testing could be performed on the second day with silicon nitride samples. Once the enzyme stocks and *E. coli* dilutions were prepared, pathogenic water cells were prepared in a well plate by adding β-gal stock, *E. coli* dilutions, and silicon nitride samples and allowing them to sit for 30 minutes at room temperature. The well plate was separated into four sections based on silicon nitride etch duration for visual comparison of colorimetric response over increasing etch times and comparison with unetched wafer samples. The initial setup of the cells with corresponding *E. coli* concentrations used and the well plate sample section designations is depicted in Figure 10.

Since samples were also cleaved into three different sizes, one well plate bioassay was constructed for each sample size.

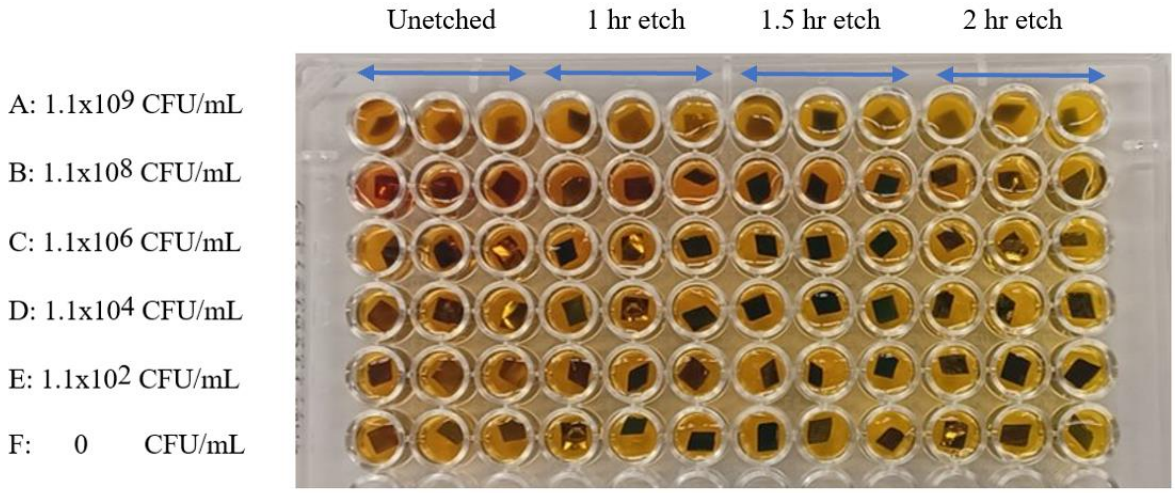

Figure 10. Well plate setup with decreasing concentrations of E. coli starting in row A with an undiluted concentration down through row F with a zero concentration; material sample separations are labeled based on etch duration. Sample sections contain three columns to indicate three replicates of each trial to ensure repeatability of results.

During this time, a SpectraMAXplus spectrophotometer shown in Figure 11 was prepared for sample readings. The spectrophotometer was calibrated with a blank cuvette and set to read absorbances for a wavelength of 575 nm, the maximum wavelength for the CPRG solution. Thirty minutes after all the components were assembled in the cells, the assay well plate was placed in the SpectraMAXplus spectrophotometer to determine color absorbance intensity, and results were recorded. A control bioassay was constructed with the same *E. coli* concentrations, β-Gal and CPRG volumes, and with three replicates but with no material present in each cell to examine the effect of silicon nitride on absorbance results and therefore analyze and determine the overall efficacy of silicon nitride as a pathogen detector in the biosensor assay.

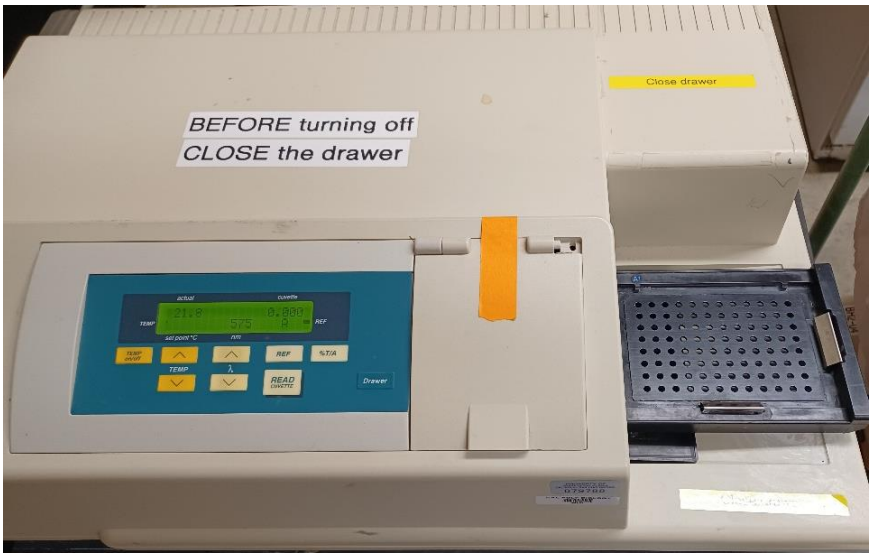

Figure 11. SpectraMAXPlus spectrophotometer from one of the Cal Poly biology laboratories.

III. Results and Data Interpretation

1. Characterization Results

A. Profilometry

The results of profilometry (see Appendix A) indicated that the etched samples were all rougher than the unetched reference wafer. The reference wafer had a 0.026 μm R_a, the 1 hr etched wafer a 0.117 μm R_a, the 1.5 hr etch had a 0.106 μm R_a, and the 2 hr etch had a 0.077 μm R_a. The expected result was that surface roughness would increase proportionally with longer etch times; however, it was instead found that none of the samples were significantly rougher in comparison with the unetched reference wafer. One theory for why this did not occur is that as the wafers were etched, the photoresist left as an etch mask on the wafer was undercut by the etchant and resulted in a relatively even etch across all samples. The etchant may have also become progressively diluted as it etches to silicon nitride, and products formed on the surface of the silicon nitride from reactions with the etchant may have interfered with deeper etching. Another possibility is that silicon nitride is too resistant to wet etching techniques—especially at the given temperature and concentration conditions of the etchant—and any changes in surface roughness were too marginal for profilometry detection.

B. Scanning Electron Microscopy (SEM)

Scanning electron microscopy (SEM) images of etched silicon nitride samples were taken in high vacuum mode and are shown in Figure 12 below.

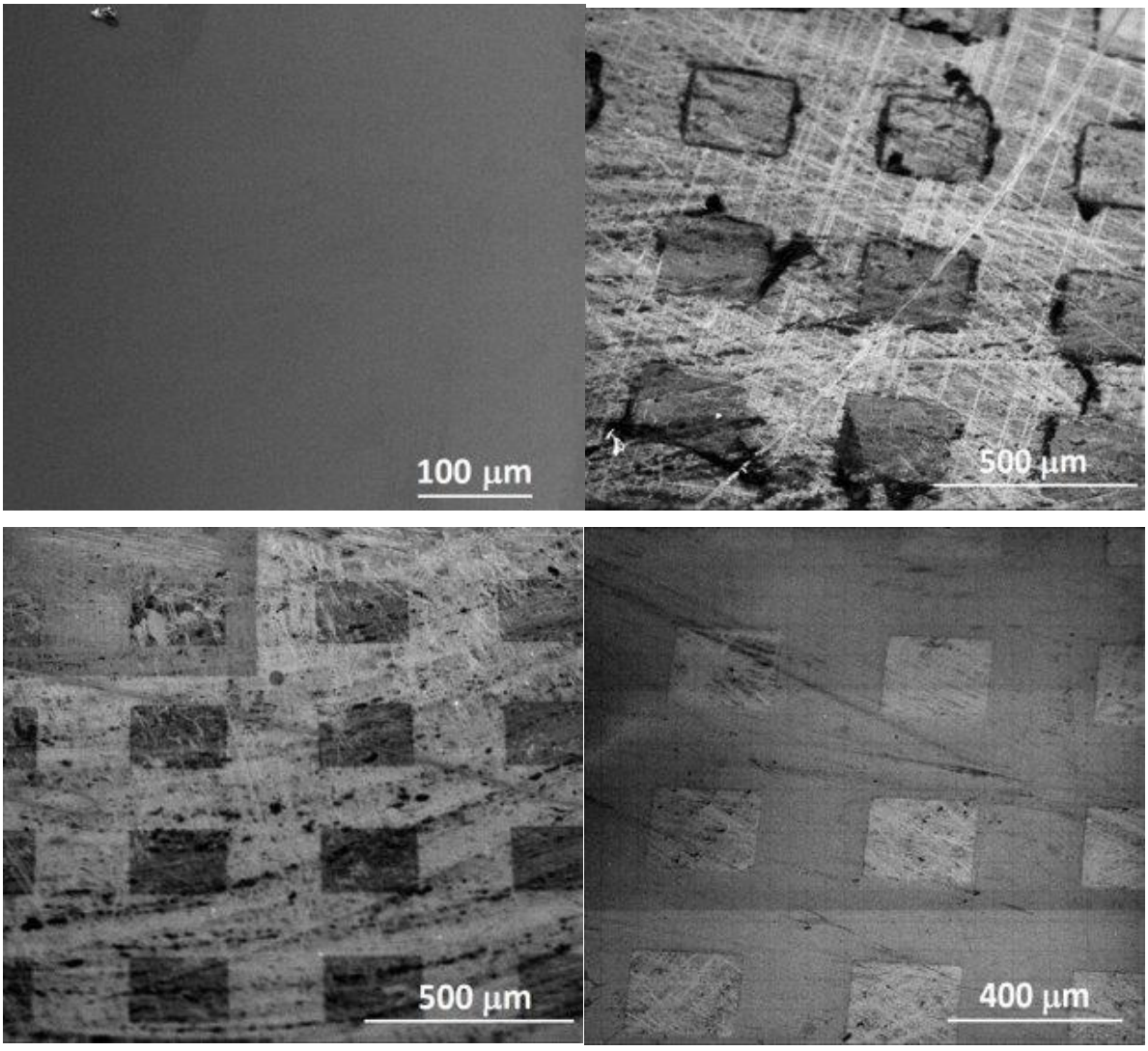

Figure 12. (Top left) SEM images of a reference silicon nitride wafer with no etch; (top right) patterned silicon nitride wafer after a 1 hr etc; (bottom left) patterned silicon nitride wafer after a 1.5 hr etch; and (bottom right) patterned silicon nitride wafer after a 2 hr etch.

As seen in Figure 12, the pattern of repeating squares from the mask was successfully imparted onto the silicon nitride layer of the wafer. The excess scratching and larger discolored sections were attributed to surface scratching due to wafer transport. The different scale length on the reference sample in comparison to the scale length on the images of the other etched samples (Figure 12) demonstrates the extreme uniformity of the reference sample. Unfortunately, etch depth differences could not be discerned between samples from the images.

C. Brunauer-Emmett-Teller (BET)

A Quantachrome Monosorb Rapid Surface Area Analyzer MS-22 was used to perform Brunauer-Emmett-Teller (BET) surface area analysis of the etched silicon nitride samples and the unetched reference sample. Measurements were repeated four times to ensure repeatability of the results (Appendix B). In comparison to the unetched reference samples, the etched wafer samples exhibited an overall increase in surface area with the 1 hr etched samples having a 42.2% increase, the 1.5 hr etched samples having a 18.4% increase, and the 2 hr etched samples having a 15.4% increase. The etched samples were expected to have increasing surface areas with larger differences for longer etch durations, but the results indicated the opposite pattern with larger differences in surface area with samples having shorter etch durations. It is hypothesized that these unexpected results are due to the step-etch process inhibiting effective etching at longer durations. Since the 2 hr etch-step was lowered into the BOE bath first, it formed products at the surface that may have inhibited etching interactions as the wafer was further lowered. Mitigation of this effect could be done by agitating the bath, adding HCl acid to remove etching products, or performing etching on separate wafers.

2. Bioassay Results

A. Visual Analysis

Visual results of the bioassay were recorded to determine the viability of silicon nitride samples in field use for colorimetric bacteria detection. Results were recorded using a Samsung Galaxy A32 8MP wide-angle camera at the same location and under the same lighting conditions since visual observation can be subjective. Initial results after CPRG was added to the cells containing all other components seemed to show a slight color gradient, but within 30 min all cells were

visually the same shade of red; results are shown in Figure 13. Based on these qualitative observations, it was determined that patterns in the colorimetric readout were visually indiscernible and not viable for detection in the field.

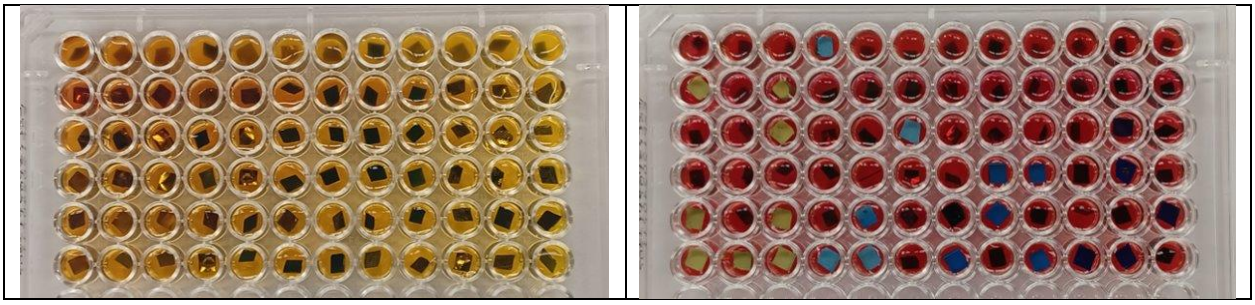

Figure 13. (Left) Initial visual results suggesting a slight color gradient; (Right) post-30 min visual results indicating no visually discernable colorimetric trends.

C. Spectrophotometry

Absorbance results of the silicon nitride bioassays were first analyzed to determine consistency of results across different sample sizes. Averages of the three repeated trials were taken for absorbance values at each *E. coli* concentration and compared across sample sizes for each sample etch type (Appendix C). Results of this comparison indicated no statistically significant difference of absorbances values between sample sizes with the same etch duration; all averaged absorbances were within 5% of one another.

Observation of the raw data from spectrophotometry indicated a consistent decline in absorbance with decreasing concentrations of *E. coli*. The single inconsistency in this trend was found in the absorbances from the undiluted *E. coli* concentration, which had absorbance values lower than absorbances from the first dilution (1.1×10^8 CFU/mL) but still higher than all other absorbance values; this trend is illustrated in Figure 14. The reason for this inconsistency is believed to be caused by the color of the TSB solution that was used only in the undiluted *E. coli* culture. All other dilutions were made in PBS, which is colorless and transparent; TSB has a slightly yellow hue that is the most likely cause of the unexpected lower absorbance values in the undiluted solutions.

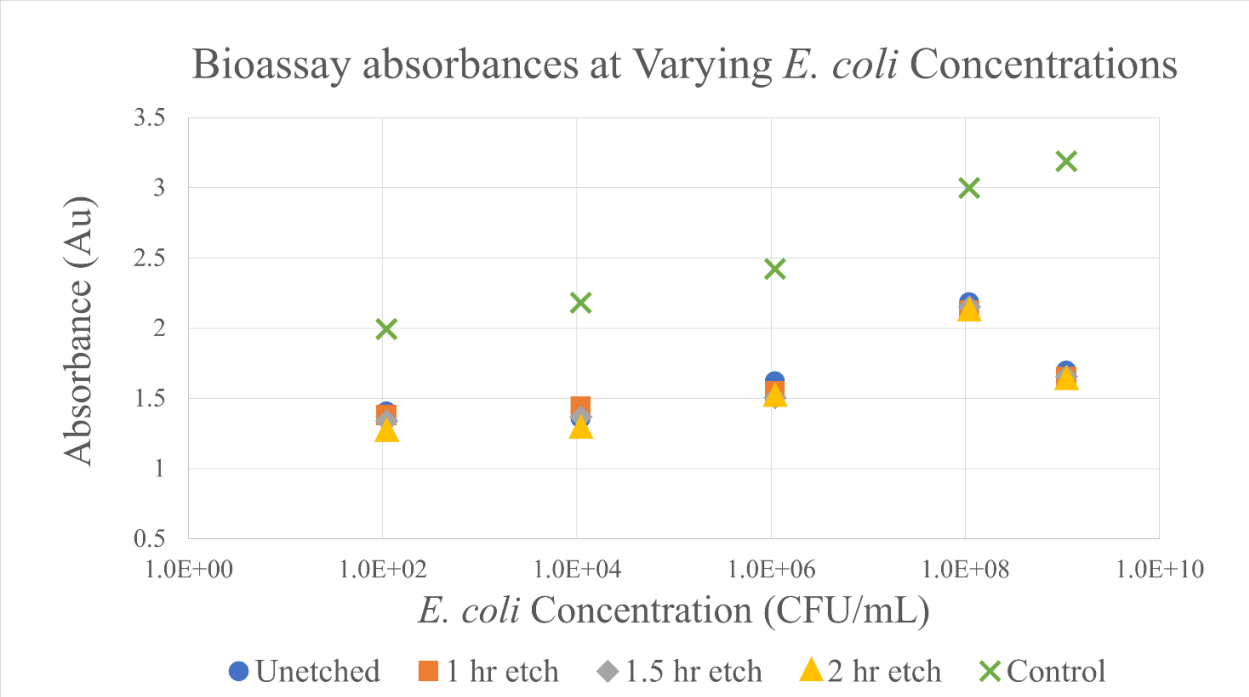

Figure 14. Absorbance of 575 nm wavelength in bioassay cells as a function of E. coli concentration.

After absorbances for the different sample sizes were found to have no statistically significant difference for a given etch duration, values across different sizes were averaged and a one-tailed t-test was performed to compare with the control bioassay that had no material present. The t-test indicated that most absorbances from the bioassays with silicon nitride were statistically different from the results of the control bioassay, suggesting that colorimetric response from enzymatic activity did occur, even though this was visually difficult to determine. Results of the t-test are displayed in Figure 15, with t-scores greater than the critical value of 2.92 indicating a 95% probability of colorimetric differences being caused by binding activity of *E. coli* and silicon nitride.

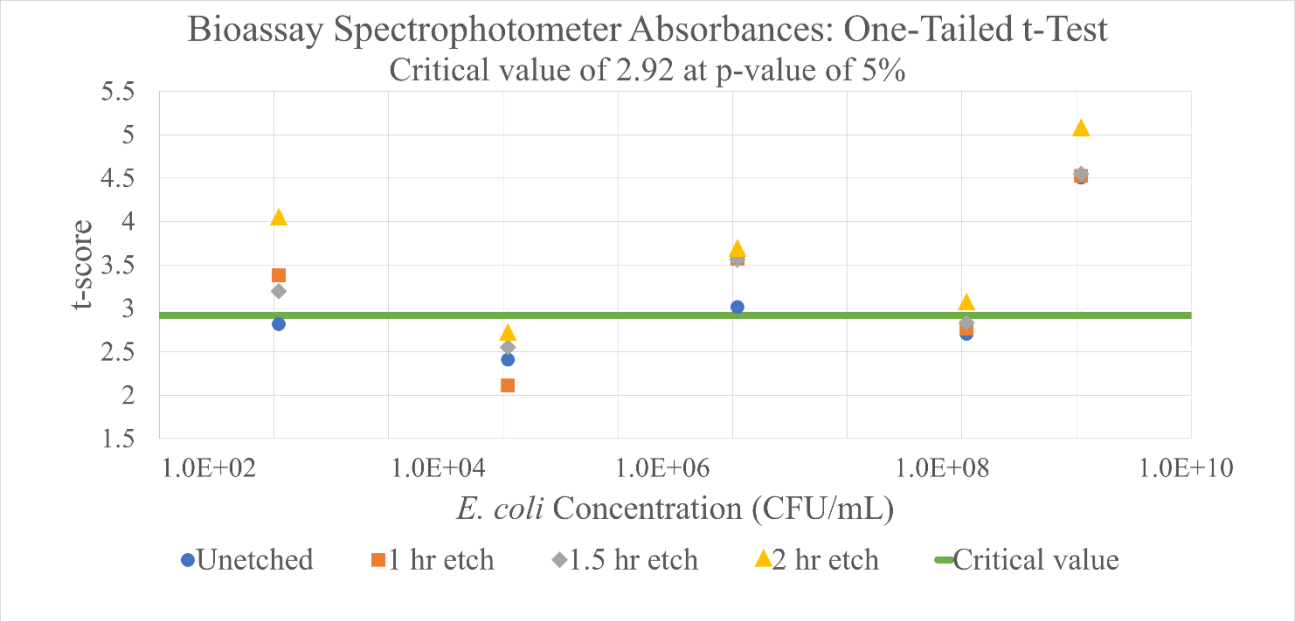

Figure 15. One-tailed t-test results comparing an average of silicon nitride bioassay absorbances with an average of control bioassay absorbances.

IV. Discussion

Characterization results show that varying etch time did not have the expected effects of increasing the surface roughness and surface area of the silicon nitride layer with increased etch duration. Surface roughness measurements indicated that although the surface roughness of etched silicon nitride samples increased compared to the unetched reference wafer, there was no significant difference between samples. BET surface area analysis results were the opposite of what was expected; although the surface area of each etched silicon nitride sample increased compared to the unetched wafer, the sample with the shortest etch duration had a significantly higher surface area increase than the other samples. Additionally, SEM imaging did not reveal noticeable etch depth differences between silicon nitride samples with different etch durations for a few possible reasons. One reason is that as the BOE etchant was not agitated during the step-etch process, unwanted etching products and the subsequent reduction in the potency of the etchant may have formed, preventing further etching on the wafer surface. Another potential cause of this may have been due to the photoresist masking layer being undercut by the etchant, which resulted in an even etch even across varying etch times. Regarding the etch depth: silicon nitride layers are different colors based on the thickness of the layer. As can be seen in Figure 7,

silicon nitride with a 1 hr etch had a light blue color, silicon nitride with a 1.5 hr etch had a dark blue color, and silicon nitride with a 2 hr etch had a bluish-purple color. According to a color chart, these correspond to thicknesses of 244 nm, 233 nm, and 225 nm, respectively (HTE Labs, 2009). SEM images were taken with tilted samples to potentially identify the silicon nitride layer, but etch depth differences could not be verified due to lack of visibility.

Overall, cleaved silicon nitride samples were found to produce a linear relationship between colorimetric readout and *E. coli* concentration: as *E. coli* concentration decreased, so did the absorbance intensity. Most of the differences were found to be statistically significant; however this was inconsistent across all data and requires further study. This proportional relationship between absorbance intensity and bacteria concentration was also qualitatively difficult to discern, and the silicon nitride fabrication methods used in this project were found to be insufficient for producing the desired exaggerated enzymatic activity that could produce results that are easily visually distinguishable for use in a field assay.

V. Future Work

Since the conditions of the selected silicon nitride etching technique produced no overall significant increase in surface roughness, it was determined that silicon nitride is resistant to low temperature and low concentration wet etching, so further investigation is required into more aggressive wet etching techniques. Additionally, it is recommended that further research be conducted into increasing temperature and etchant concentration to examine their effects on surface roughness and area of samples. Physical etching techniques should also be examined, such as reactive ion etching (RIE).

Visual results and statistical analysis using the one-tailed t-test indicated a need for more exaggerated enzymatic activity that would be viable for a field assay. A possible reason silicon nitride did not produce exaggerated colorimetric responses is that the IEP of silicon nitride is too close to the neutral pH of water, resulting in a moderate positive charge. Further research should be conducted to study the colorimetric responses of different materials deposited onto a silicon substrate with varying IEP values to measure the corresponding colorimetric response.

One advantage of the cleaved silicon nitride samples over nanoparticles is that they can be recovered and reused in more assays, further adding to their low-cost benefit. This process was briefly examined in a preliminary recovery experiment, where the 5 mm x 4 mm samples were removed from their assay, soaked overnight for 24 hours in a 10% by volume bleach solution, and then autoclaved at 121ºC for 20 minutes. The bioassay experiment was conducted again with the recovered samples, and it was found that averaged absorbance values exhibited a difference of only 2.56% in comparison to the initial results before recovery (Appendix D). This indicates high promise for the recovery and reuse of silicon nitride in the detection of pathogens in water.

VI. Conclusions

Silicon nitride is a promising material for future inexpensive bacteria-detecting bioassays. Despite limitations encountered in wafer etching and processing, preliminary results indicated a proportional trend in colorimetric absorbance values with decreasing bacteria concentrations. Further investigation into the effects of wet etching temperature and concentration as well as different etch methods could produce samples that more consistently produce exaggerated absorbance values that can be used to both qualitatively and quantitatively identify bacteria concentrations. Preliminary results of recovery and reuse of samples show that inexpensive, reusable bioassays are possible if reliable sample processing can be established.

VII. References

Ahmadian, A.; Ehn, M.; and Hober, S. Pyrosequencing: History, biochemistry and future. *Clin. Chim. Acta* 2006, 363, 83–94.

Annan, Kofi (2003, May 16). *'Water-Related diseases responsible for 80 percent of all illnesses, deaths in developing world,' says Secretary-General in Environment Day Message.* United Nations Meetings Coverage and Press Releases. https://www.un.org/press/en/2003/sgsm8707.doc.htm

Berry, V.; Gole, A.; Kundu, S.; Murphy, C. J.; and Saraf, R. F. J. (2005). Deposition of CTAB-terminated nanorods on bacteria to form highly conducting hybrid systems. *American Chemical Society*, 127, 17600.

Burham, N.; Sugandi, G.; Nor, M.; Majlis, B. (2016). Effect of temperature on the etching rate of nitride and oxide layer using Buffered Oxide Etch. 516-519. doi: 10.1109/ICAEES.2016.7888099.

Chuang, N.-N. and Yang, B.-C. (1990). A sialidase from the hepatopancreas of the shrimp *penaeus japonicus* (*crustacea: Decapoda*): Reversible binding with the acidic beta-galactosidase. *Comparative Biochemistry and Physiology Part C: Comparative Pharmacology*, *97*(2), 353–356. https://doi.org/10.1016/0742-8413(90)90153-z

U.S. Food and Drug Administration. "Bad Bug Book, Foodborne Pathogenic Microorganisms and Natural Toxins." 2nd ed. Silver Spring, MD: US Food and Drug Administration; 2012.

Halbleiter (2021). *Semiconductor technology from A to Z*. Doping: n- and p-semiconductors - Fundamentals - Semiconductor Technology from A to Z – Halbleiter, retrieved November 2021, from https://www.halbleiter.org/en/fundamentals/doping/.

Hitachi High-Tech Corporation. (2021). *The Semiconductor Material Silicon*. 3. The semiconductor material silicon: Hitachi High-Tech GLOBAL, retrieved from November 2021, from https://www.hitachi-hightech.com/global/products/device/semiconductor/silicon.html.

Holmes, Jonathan. How much does silicon cost? Cement Answers, retrieved March 2022, from https://cementanswers.com/how-much-does-silicon-cost/

HTE Labs. (July 6, 2009). Si_3N_4 color chart for LPCVD grown silicon nitride, retrieved May 25, 2022, from http://www.htelabs.com/appnotes/si3n4_color_chart_LPCVD_silicon_nitride.htm

Iqbal, S.S.; Mayo, M.W.; Bruno, J.G.; Bronk, B.V.; Batt, C.A.; and Chambers, J.P. (2000). A review of molecular recognition technologies for detection of biological threat agents. *Biosensors and Bioelectronics*, 15, 549–578.

Ji, J.; Schanzle, A.; and Tabacco, M. B. (2004). Real-Time Detection of Bacterial Contamination in Dynamic Aqueous Environments Using Optical Sensors. *Analytical Chemistry*, 76, 1411.

Juers, D. H.; Matthews, B.W.; and Huber R. E. (2012). LacZ ß-galactosidase: Structure and function of an enzyme of historical and molecular biological importance. *Protein Sci*, 21(12), 1792-1807. doi: 10.1002/pro.2165.

Leber, M.; Shandhi, M. M. H.; Hogan, A.; Solzbacher, F.; Bhandari, R.; and Negi, S. (March 1, 2016). Different methods to alter surface morphology of high aspect ratio structures. *Allied Surface Science*, 365, 180-190. doi: 10.1016/j.apsusc.2016.01.008

Lewis, J. A. (2004). Colloidal processing of ceramics. *Journal of the American Ceramic Society*, *83*(10), 2341–2359. https://doi.org/10.1111/j.1151-2916.2000.tb01560.x

Liang, X.; Liao, C.; Thompson, M. L.; Soupir, M. L.; Jarboe, L. R.; and Dixon, P. M. (2016). *E. coli* surface properties differ between stream water and sediment environments. *Frontiers in Microbiology, 7*. https://doi.org/10.3389/fmicb.2016.01732

Mandal, P.K.; Biswas, A.K.; Choi, K.; and Pal, U.K (2011). Methods for rapid detection of foodborne pathogens: An overview. *Am. J. Food. Technol.*, 6, 8–102.

Miranda, O. R. *et al.* (2011). Calorimetric Bacteria Sensing Using a Supramolecular Enzyme-Nanoparticle Biosensor. *Journal of the American Chemical Society*, 133, 9650-9653. doi.org/10.1021/ja2021729

Monex (2021). *MONEX Live Gold Spot Prices.* MONEX Precious Metals, retrieved November 2021, from https://www.monex.com/gold-prices/

Okamoto, H. (2005). N-si (nitrogen-silicon). *Journal of Phase Equilibria & Diffusion*, *26*(3), 293–294. https://doi.org/10.1361/15477030523571

Ramirez-Castillo, F. Y. *et al.* (2015). Waterborne Pathogens: Detection Methods and Challenges. *Pathogens*, 4, 307-334. doi:10.3390/pathogens4020307

Riley, F. L. (2004). Silicon nitride and related materials. *Journal of the American Ceramic Society*, *83*(2), 245–265. https://doi.org/10.1111/j.1151-2916.2000.tb01182.x

ThermoFisher. (2021). *Fluorescence In Situ Hybridization (FISH)*. ThermoFisher-US, retrieved March 2022, from https://www.thermofisher.com/us/en/home/life-science/cell-analysis/cellular-imaging/in-situ-hybridization-ish/fluorescence-in-situ-hybridization-fish.html

van der Maaden, K.; Tomar, J.; Jiskoot, W.; and Bouwstra, J. (2014). Chemical modifications of silicon surfaces for the generation of a tunable surface isoelectric point. *Langmuir*, *30*(7), 1812–1819. https://doi.org/10.1021/la404654t

Wang, S.; Zhang, Y.; Liu, J.; Zou, X.; and Zhang, J. (2019). PECVD SiO_2/Si_3N_4 double-layer electrets for application in Micro-devices. *IOP Conference Series: Materials Science and Engineering*, *611*(1), 012088. https://doi.org/10.1088/1757-899x/611/1/012088

Woolhouse, M.E.J. (2006). Where Do Emerging Pathogens Come from? *Microbe-Emerging Paths*, 1, 511-515.

World Health Organization (June 14, 2019). Drinking-Water. World Health Organization, retrieved November 2021, from https://www.who.int/news-room/fact-sheets/detail/drinking-water

Zhou, J. (2003). Microarrays for bacterial detection and microbial community analysis. *Current Opinion in Microbiology*, 6, 288–294.

VIII. Appendix

Appendix A

Profilometry Measurements (μm)

Table A.1: Surface Roughness Measurements of Unetched and Etched Wafers

Wafer	Trial 1,1	Trial 1,2	Trial 1,3	Trial 1,4	Trial 1,5	Average Ra
Unetched	0.02	0.01	0.03	0.02	0.04	0.024
2 hr Etch	0.06	0.06	0.1	0.04	0.03	0.058
1.5 hr Etch	0.11	0.09	0.07	0.06	0.08	0.082
1 hr Etch	0.12	0.07	0.13	0.11	0.16	0.118
Wafer	**Trial 2,1**	**Trial 2,2**	**Trial 2,3**	**Trial 2,4**	**Trial 2,5**	**Average Ra**
Unetched	0.06	0.01	0.02	0.02	0.05	0.032
2 hr Etch	0.11	0.09	0.12	0.13	0.06	0.102
1.5 hr Etch	0.11	0.14	0.12	0.12	0.16	0.13
1 hr Etch	0.1	0.14	0.14	0.11	0.13	0.124
Wafer	**Trial 3,1**	**Trial 3,2**	**Trial 3,3**	**Trial 3,4**	**Trial 3,5**	**Average Ra**
Unetched	0.03	0.02	0.04	0.02	0.01	0.024
2 hr Etch	0.08	0.09	0.06	0.07	0.06	0.072
1.5 hr Etch	0.12	0.1	0.09	0.14	0.08	0.106
1 hr Etch	.11	0.13	0.11	0.1	0.1	0.11

Appendix B

Brunauer-Emmett-Teller (BET) Measurements

Table B.1: Raw and Averaged Surface Area Measurements with Calculated Percent Difference

	Unetched	1 hr Etched	1.5 hr Etched	2 hr Etched
Mass (g)	0.0324	0.0231	0.0285	0.0288
	0.0323	0.0232	0.0247	0.0291
	0.0323	0.0232	0.0247	0.0291
	0.0323	0.0232	0.0247	0.0291
AVERAGE	0.0323	0.0232	0.0257	0.0290
Surface Area (m^2)	18.42	18.78	17.06	19.25
	20.81	19.56	17.05	20.78
	20.28	22.73	21.72	22.46
	22.92	22.99	23.62	22.95
AVERAGE	20.61	21.02	19.86	21.36
Specific Surface Area (m^2/g)	568.52	812.99	598.60	668.40
	644.27	843.10	690.28	714.09
	627.86	979.74	879.35	771.82
	709.60	990.95	956.28	788.66
AVERAGE	637.56	906.70	781.13	735.74
% Increase from Unetched	--	42.21%	18.38%	15.40%

Appendix C

Sample Size Correlations for Etch Groups

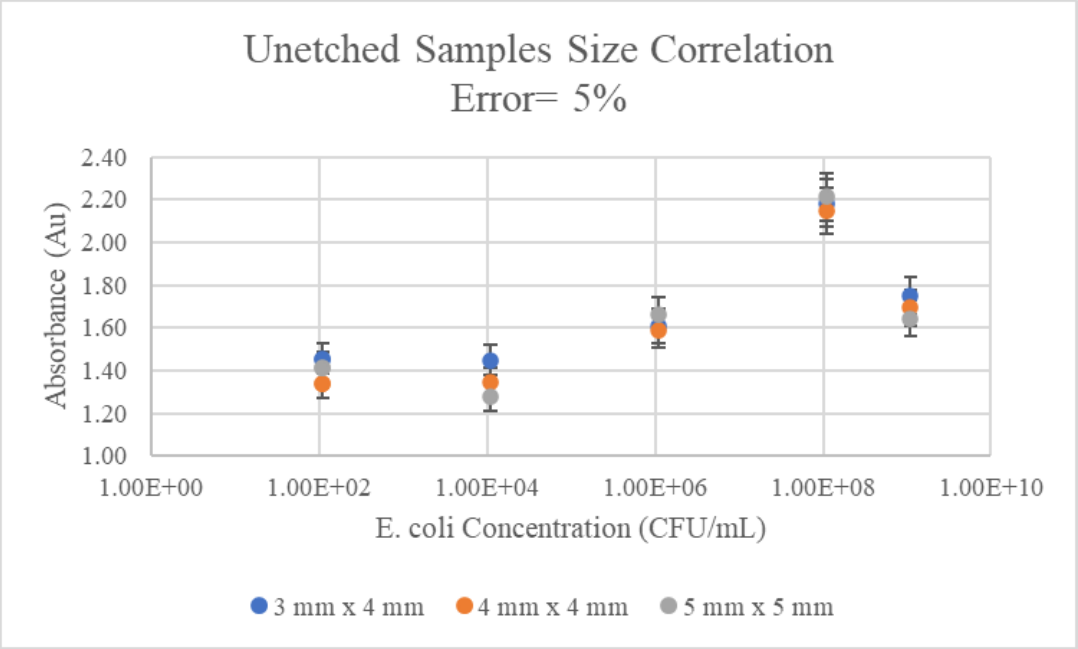

Figure C.1. Correlation of absorbances between different sample sizes for unetched wafer; data points within 5% deviation of one another.

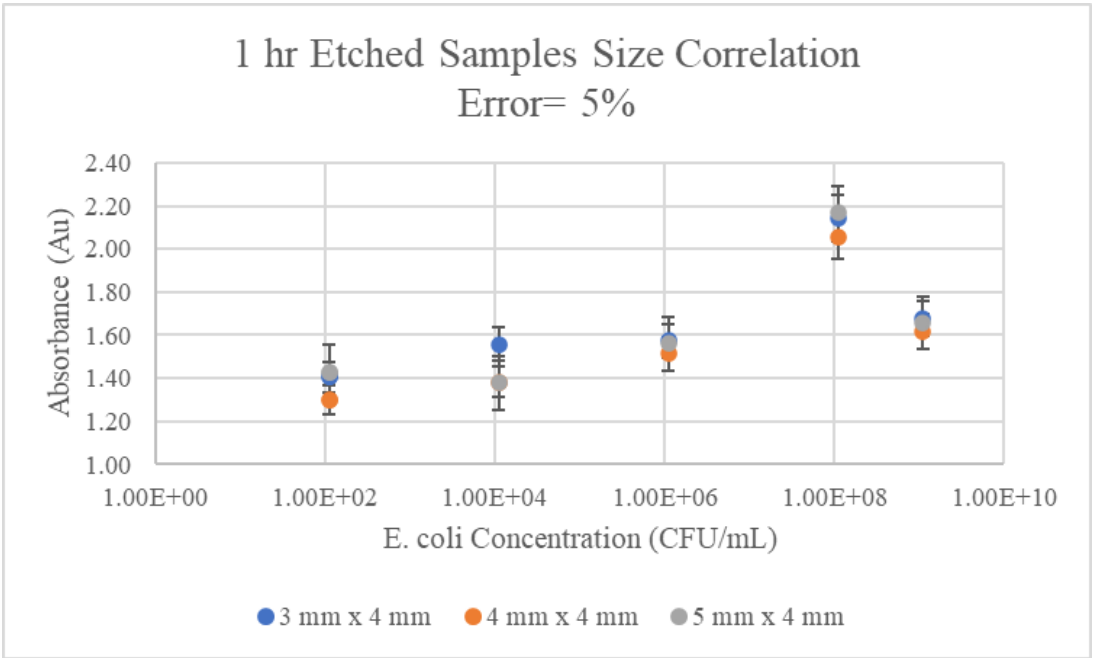

Figure C.2. Correlation of absorbances between different sample sizes for 1 hour etched wafer; data points within 5% deviation of one another.

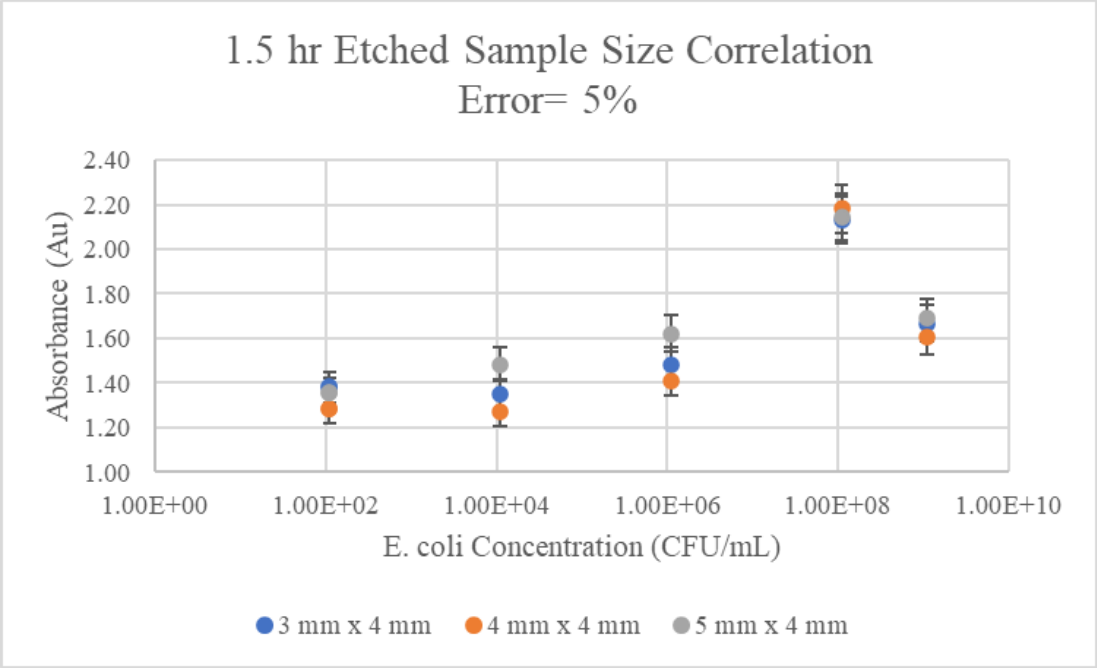

Figure C.3. Correlation of absorbances between different sample sizes for 1.5 hour etched wafer; data points within 5% of one another.

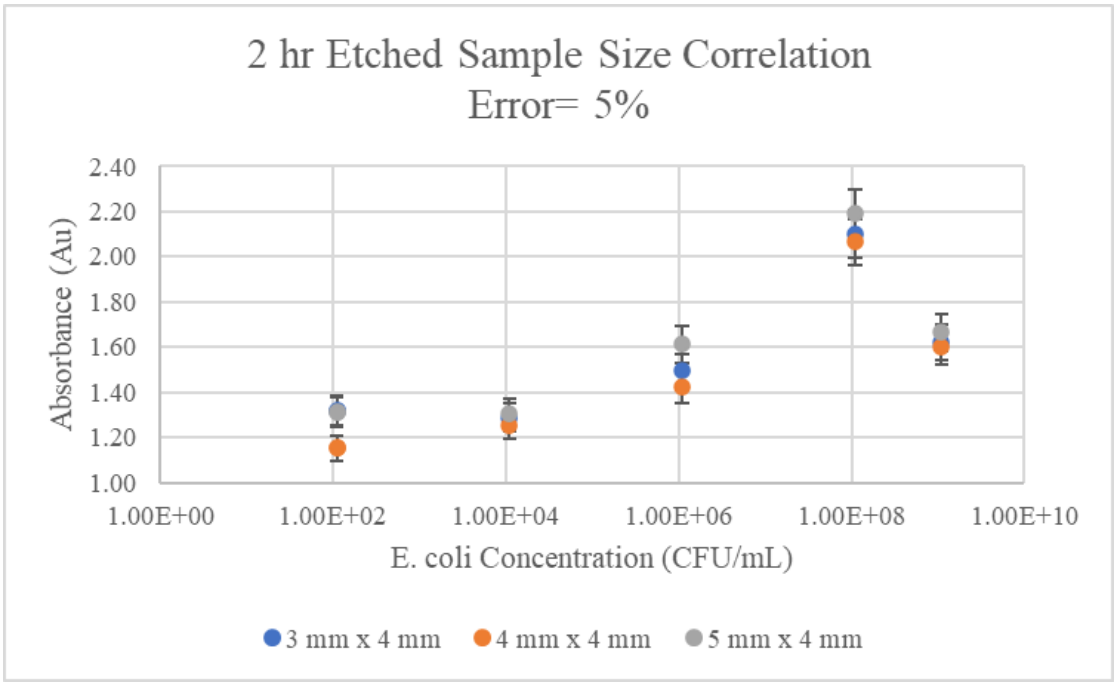

Figure C.4. Correlation of absorbances between different sample sizes for 2 hour etched wafer; data points within 5% of one another.

Appendix D

Recovery Experiment Results

Samples from the 5 mm x 4 mm sample size assay were recovered from their well plate and placed in 200 µL of a 10% by volume bleach solution overnight for 24 hours. The following day, samples were rinsed twice in deionized water to ensure removal of bleach solution, and subsequently autoclaved at 121°C for 20 minutes. After recovery, the samples were used again in a bioassay experiment and spectrophotometry was used to measure absorbance values to compare with the initial results of the samples before recovery.

Table D.1: Averaged Absorbances of Initial and Post-Recovery 5 mm x 4 mm samples

Concentration (CFU/mL)	Initial				Post-Recovery			
	Unetched	1 hr Etch	1.5 hr Etch	2 hr Etch	Unetched	1 hr Etch	1.5 hr Etch	2 hr Etch
1.10E+09	1.6453	1.6573	1.6910	1.6650	1.8570	1.8080	1.8480	1.9230
1.10E+08	2.2127	2.1687	2.1453	2.1893	1.5640	1.5080	1.4520	1.4940
1.10E+06	1.6610	1.5610	1.6210	1.6120	1.6490	1.6260	1.6880	1.6600
1.10E+04	1.2753	1.3780	1.4840	1.3070	1.6580	1.6420	1.5410	1.6500
1.10E+02	1.4147	1.4310	1.3580	1.3150	1.6330	1.5420	1.6410	1.6920
0.00	1.4927	1.3773	1.3543	1.3173	1.6380	1.7500	1.6420	1.6010

Table D.2: Averaged Percent Differences of Initial and Post-Recovery Absorbances for 5 mm x 4 mm samples

Concentration (CFU/mL)	% Difference				
	Unetched	1 hr Etch	1.5 hr Etch	2 hr Etch	AVERAGE
1.10E+09	11.40%	8.33%	8.50%	13.42%	10.41%
1.10E+08	-41.47%	-43.81%	-47.75%	-46.54%	-44.89%
1.10E+06	-0.73%	4.00%	3.97%	2.89%	2.53%
1.10E+04	23.08%	16.08%	3.70%	20.79%	15.91%
1.10E+02	13.37%	7.20%	17.25%	22.28%	15.02%
0.00	8.87%	21.30%	17.52%	17.72%	16.35%
					2.56%